Available online at www.sciencedirect.com
ScienceDirect
Applied Catalysis B: Environmental 82 (2008) 89–102
APPLIED CATALYSIS B: ENVIRONMENTAL
www.elsevier.com/locate/apcatb

Influence of Sn content on PtSn/C catalysts for electrooxidation of C_1–C_3 alcohols: Synthesis, characterization, and electrocatalytic activity

Jae Hong Kim [a], Sung Mook Choi [a], Sang Hoon Nam [a], Min Ho Seo [a], Sun Hee Choi [b], Won Bae Kim [a,*]

[a] *Department of Materials Science and Engineering, Gwangju Institute of Science and Technology (GIST), 261 Cheomdan-gwagiro, Buk-gu, Gwangju 500-712, South Korea*
[b] *Pohang Accelerator Laboratory, San-31 Hyoja-dong, Pohang, Kyungbuk 790-984, South Korea*

Received 15 August 2007; received in revised form 15 January 2008; accepted 15 January 2008
Available online 20 January 2008

Abstract

A series of carbon-supported bimetallic PtSn catalysts for the electrooxidation of C_1–C_3 alcohols (i.e., methanol (C_1), ethanol (C_2), and 1-propanol (C_3)) were prepared with different Pt:Sn atomic ratios using borohydride reduction method combined with freeze-drying procedure at room temperature. The catalysts were investigated by employing various physicochemical analyses: X-ray diffraction (XRD), transmission electron microscopy (TEM) and extended X-ray absorption fine structure (EXAFS) to investigate the structural modification, and X-ray photoelectron spectroscopy (XPS) and X-ray absorption-near-edge spectroscopy (XANES) to characterize the change in electronic features. The variation of Sn content by forming PtSn alloys causes significant structural and electronic modifications of Pt crystallites, resulting in increases of lattice parameter and decreases of the Pt 5d band vacancies with Sn content. Cyclic voltammetry (CV) measurements showed that the addition of Sn into the Pt catalyst promotes the electro-catalytic activities for the electrooxidations of C_1, C_2, and C_3 alcohols, in which the maximum activities appeared at different Sn contents for the C_1–C_3 alcohols. In particular, a shift in optimum Pt:Sn composition was observed in that the Sn content required to reach the maximum peak current density was increased with the increasing number of carbon atoms in the C_1–C_3 alcohols. Both the geometric and electronic effects with variation of Sn content are in close relationship in the bimetallic PtSn catalysts, consequently affecting the electrocatalytic activities by showing volcano-type behaviors over the electrooxidation of the individual alcohol.

Keywords: PtSn catalyst; Electrooxidation; Methanol; Ethanol; 1-propanol; Fuel cells; Biomass

1. Introduction

Direct alcohol fuel cells (DAFCs) operating with $C_{x\geq 2}H_yO_z$ liquid fuel types at low temperatures (<100 °C), whose oxygenated hydrocarbons can be derived from biomass [1–4], have been considered to be a potential alternative to direct methanol fuel cell (DMFC) with advantages of renewable use of the liquid fuels and theoretically higher energy density, and lower toxicity. Thus, aliphatic alcohols, such as ethanol [2,5–13], ethylene glycol [11,12], and propanol [14] have recently been examined as promising fuels for DAFCs. Overall reaction of anodic electrooxidation of the oxygenated hydrocarbon in an acidic aqueous medium is represented below, which takes place in a Pt-based catalyst electrode of a proton exchange membrane (PEM) fuel cell:

$$C_{x\geq 2}H_yO_z + (2x - z)H_2O \rightarrow xCO_2 + (4x + y - 2z)H^+ + (4x + y - 2z)e^-$$

From a kinetic point of view, the anodic reaction is sluggish at moderate operating temperatures of the PEM type fuel cells because complex reaction steps are involved during the complete oxidation reaction; for instance, multi-electron transfers should undergo together with consecutive adsorption/surface reactions/desorption of several reaction products and byproducts. In addition, some of poisoning species (e.g., CO), which are produced during the electrooxidation of alcohols, are irreversibly adsorbed on the surface active sites of the Pt-based catalysts, thereby impeding the electrocatalysts from catalytically working. Even the simplest alcohol, i.e.

* Corresponding author. Tel.: +82 62 970 2317; fax: +82 62 970 2304.
E-mail address: wbkim@gist.ac.kr (W.B. Kim).

0926-3373/$ – see front matter © 2008 Elsevier B.V. All rights reserved.
doi:10.1016/j.apcatb.2008.01.011

methanol (CH_3OH), its complete anodic oxidation ($CH_3OH + H_2O \rightarrow CO_2 + 6\ H^+ + 6e^-$) involves six electrons so that the oxidation occurs via multi-steps with several products or reaction intermediates such as formaldehyde and formic acid. The complete electrooxidation of the higher alcohols having C–C bonds is therefore much more complicated than that of methanol since additional activation energies are necessary for scission of C–C bond and oxidative removal of much larger quantity of C_1- and C_2-type intermediates, especially at low temperatures (20–120 °C) [15].

Despite platinum is generally known to be one of the best electrocatalyst for low temperature operating PEM type fuel cells, it still has intrinsic drawbacks such as high price, limited capability for C–C bond scission and vulnerability toward ''poisoning'' by CO or carbonaceous intermediates. To improve the electrocatalytic activity, modifications of Pt nanocrystallites have been tried by alloying with other elements such as Ru [16], Sn [11,17,18], or Au [19]. Bimetallic alloy formation changes structural and electronic properties of Pt-based electrocatalysts, allowing desired reaction pathways with lower activation energy via tuning energies of adsorption, surface reactions, and/or desorption reaction on the surface, and facilitating to produce oxygenated species from water decomposition at low potentials for the oxidation of carbonaceous intermediates formed on the catalyst surface [15,20,21].

In this study, we investigate that how the systematic modification of the PtSn/C catalysts on their structural and electronic features by adding Sn content from 0 to 50 wt.% can correspond to their catalytic activities for the electrooxidations of methanol (C_1), ethanol (C_2), and 1-propanol (C_3). These alcohols were selected as the simple model molecules to study biomass-derived oxygenated hydrocarbons [1] (e.g., ethanol, ethylene glycol, glycerol, sorbitol, glucose, and etc.) as the potential fuels in DAFC at low temperatures, because C_1–C_3 alcohols chosen here contain basic bonding units of the oxygenated hydrocarbons like C–H, C–O, and O–H bonds with different number of C–C bonds. The catalysts were investigated by several physicochemical analyses: X-ray diffraction (XRD), transmission electron microscopy (TEM) and extended X-ray absorption fine structure (EXAFS) to investigate structural modification, together with X-ray photoelectron spectroscopy (XPS) and X-ray absorption-near-edge spectroscopy (XANES) to characterize electronic properties. The relationship between their physico-chemical properties and electrocatalytic activities will be explored and discussed with respect to variation of Sn content for the electrooxidation of the individual C_1, C_2, and C_3 alcohol, respectively.

2. Experimental

2.1. Preparation of carbon-supported bimetallic PtSn catalysts

All carbon-supported 20 wt.% Pt and PtSn catalysts were synthesized using borohydride reduction method combined with freeze-drying procedure. Carbon support used in this study was Vulcan XC-72R (Cabot Corp., $S_{BET} = 236.8\ m^2g^{-1}$). Pt salt ($H_2PtCl_6{\cdot}xH_2O$, Aldrich) and Sn salt ($SnCl_2{\cdot}2H_2O$, Aldrich) were used as precursors for the PtSn catalysts. The carbon black powder was ultrasonically dispersed in 200 cm^3 of triply de-ionized Millipore water (18 MΩ cm) until the solution pH was around 12 with sodium carbonate (Na_2CO_3, Aldrich). The calculated amount of Pt and Sn salts was added to the carbon-suspended solution and mixed with vigorous stirring. The pH value of the solution was then adjusted to around 12 again with Na_2CO_3. The metal ions were reduced by dropwise addition of 50 cm^3 of a freshly prepared 0.5 M aqueous $NaBH_4$ solution (Aldrich) over 1 h with a syringe pump (KD Scientific Inc.). The used amount of reducing agent $NaBH_4$ was 4 times greater than that of the exact stoichiometry to ensure sufficient reduction of the metal salts. The resulting slurries were filtered at 2 h after all of the $NaBH_4$ was added and the filtered cake was then washed thoroughly with the Millipore de-ionized water (18 MΩ cm) and dried by the freeze-drying method without any heat treatment.

Table 1 summarizes chemical composition of the carbon-supported Pt and PtSn catalysts prepared in this study through elemental analysis and surface composition analysis from XPS. The nominal metal loading on the carbon was fixed to 20 wt.% (w/w) metal (Pt + Sn) on the carbon support, but actual metal loadings determined by inductively coupled plasma – atomic emission spectroscopy (ICP-AES) were resulted in around 17 wt.% (Pt + Sn) compared to the carbon support, suggesting all the homemade PtSn/C catalysts were prepared in a controlled manner. For the ICP-AES analyses, the freshly prepared 20 mg catalysts were introduced into a 60 ml Teflon-made digestion vessel (Savillex, USA), and mixed with a solution mixture containing 4 ml aqua regia (37% HCl 3 ml + 70% HNO_3 1 ml),

Table 1
Quantitative composition analysis of the 20 wt.% metal-loaded Pt/C and PtSn/C catalysts

Catalyst	Metal loading[a] (wt.%)		Nominal Pt/Sn (atomic ratio)	Pt/Sn[a] (atomic ratio)	Pt/Sn[b] (atomic ratio)
	Pt	Sn		From ICP	From XPS
Pt/C	17.5	–	–	–	–
Pt4Sn1/C	14.4	2.4	4.0	3.64	2.63
Pt3Sn1/C	12.3	4.4	3.0	1.70	1.48
Pt2Sn1/C	11.2	6.2	2.0	1.10	1.08
Pt3Sn2/C	10.1	7.1	1.5	0.87	0.55
Pt1Sn1/C	7.9	8.3	1.0	0.58	0.50

[a] Chemical composition determined by ICP-AES analysis.
[b] Surface atomic ratio calculated from XPS by using peak areas normalized on the basis of sensitivity factors [22].

0.5 ml HF (50%), and 0.5 ml $HClO_4$ (70%). The vessel had been digested at 150 °C with a pressure of *ca.* 80 psi for several days until a yellowish homogenous liquid solution has been observed. After cooling the vessel to room temperature, 1% HCl solution was added to make samples for the ICP-AES measurements using an OPTIMA 4300 DV model (PerkinElmer, USA). All catalysts were denoted as Pt_xSn_y/C, where the subscript denotes nominal atomic ratio of Pt to Sn.

2.2. Physicochemical characterizations

X-ray diffraction (XRD) analyses were carried out with Rigaku Rotalflex (RU-200B) X-ray diffractometer using Cu Kα (λ = 1.5405 Å) source with a Ni filter to identify alloy formation and characterize the structural change of the PtSn crystallite. The source was operated at 40 kV and 100 mA. The 2θ angular region between 15° and 85° was explored at a scan rate of $3^\circ\,min^{-1}$. A second fine scan with a scan rate of $0.05^\circ\,min^{-1}$ from 60° to 75° was carried out to obtain a detailed (2 2 0) diffraction peak of the crystallite and the (2 2 0) peak was fitted using the Gaussian function in order to calculate average particle size and lattice parameters. For all XRD measurements, the resolution in the 2θ scans was kept at 0.02°.

The morphologies of Pt and PtSn particles were investigated using a JEOL JEM-2100 transmission electron microscope operated at 200 kV. All TEM samples were prepared by ultrasonically suspending the catalyst particles in an ethanol solution. Drops of the suspension were deposited onto a standard Cu grid (200-mesh) covered with a carbon film and dried for 20 min to allow ethanol and water to evaporate, leaving catalyst particles dispersed on the grid prior to being inserted into the microscope. More than 100 different particles visible on the micrographs were employed to estimate average particle size. The arithmetic mean particle diameter, d, is calculated from following equation:

$$d = \frac{\Sigma n_i d_i}{\Sigma n_i},$$

where n_i is the frequency of the catalyst particles having diameter of size d_i.

The chemical states and surface compositions of Pt and Sn were analyzed by X-ray photoelectron spectroscopy (XPS, ESCALAB 250, UK) with a monochromic Al Kα X-ray source (E = 1486.6 eV). The catalyst powders were attached to a sample holder using a small piece of carbon tape. No significant charging effects were detected. Data processing was performed with XPSPEAK software program. The background was corrected using the Shirley method, and the binding energy (BE) of C 1s peak from the support at 284.5 eV was taken as an internal standard. The Pt:Sn surface atomic ratios were calculated from peaks areas normalized by published atomic sensitivity factor of the corresponding element [22]. Peak areas were estimated by calculating the integral of each peak after subtracting a Shirley background and fitting the experimental peak by a combination of Lorenzian/Gaussian (L/G) curves of a variable proportion.

X-ray absorption measurements were conducted on 7C and 3C1 beamlines of Pohang Accelerator Laboratory (PAL; 2.5 GeV with the stored currents of 130–180 mA), Korea. A Si (1 1 1) double crystal monochromator was employed to monochromatize the X-ray photon energy. The incident beam intensity was monitored using an ionization chamber purged with a gas mixture of N_2 (80%) and Ar (20%), and the transmitted beam intensity was measured in an ionization chamber filled with a pure N_2 flow. The spectra were taken at room temperature in a transmission mode for L_{III}-edge of Pt (11564 eV) under the ambient condition. Higher order harmonic contamination was eliminated by detuning the monochromator to reduce the incident X-ray intensity by about 30%. Energy calibration was performed using a standard metal foil.

The X-ray absorption near-edge spectra were analyzed using the IFEFFIT software programs [23,24]. The pre-edge background was removed in a pre-edge region of 11414–11514 eV with a straight line and subtracted the extrapolated values from the entire spectrum. The resulting elemental absorption was then normalized by using atomic-like absorption at the edge. The white line (WL) areas of Pt L_{III} edge were calculated by adopting an arctangent step and by fitting a Lorentzian function to the WL curve in the region from −50 to 100 eV. The extended X-ray absorption fine structure (EXAFS) data for the PtSn/C catalysts were analyzed using with the IFEFFIT programs [23,24] and the FEFF 8.4 code [25]. The interference function of the EXAFS data is defined as $\chi(E) = (\mu(E) - \mu_0(E))/\Delta\mu_0\ (E_0)$ above the absorption edge E_0, where $\mu(E)$ is the absorption coefficient due to the particular edge of the element in sample, $\mu_0(E_0)$ is the atomic-like absorption, and $\Delta\mu_0(E_0)$ is the jump at the edge step. The post-edge background function $\mu_0(E)$ is approximated by a piecewise spline that can be adjusted, so that low-R components of the Fourier-transformed data $\chi(R)$ are optimized. The power-scale EXAFS function $k^3\chi(k)$ in the momentum k space was Fourier-transformed to obtain the radial structural function (RSF) of the samples [26]. For Fourier transformation, k_{min} and k_{max} were chosen in the range of 2.3–2.8 and 12.0–13.0 $Å^{-1}$ for Pt EXAFS, respectively. A Hanning window sill was used to reduce the truncation effect from the transformation over a finite range. The nonlinear EXAFS fitting was performed in R-space without Fourier filtering over the region of 1.8–3.1 Å. The theoretical standard for Pt–Pt and Pt–Sn single scattering were synthesized with the FEFF code using structural information for Pt metal [27,28]. A single adjustable parameter in the EXAFS analysis of the amplitude reduction factor S_0^2 was taken to be 0.80 for Pt, which was found by fitting the experimental RDF of Pt foil with the theoretical one. Since the number N of the following equation was calculated to be 8.3 in this work, where Δk and ΔR are the k- and R-ranges, and the Debye–Waller factor (σ^2) and energy shift (ΔE) of Pt–Sn scattering can be assumed to those of Pt–Pt scattering [29], we could fit the EXAFS functions with seven variables to show small r-factors (see Table 3)

$$N \approx \frac{2\Delta k \Delta R}{\pi}$$

2.3. Electrooxidation activity measurements

Electrocatalytic activities towards alcohol oxidations were measured over a three-electrode cell at 298 K (±1 K) by cyclic voltammetry (CV) method using EG&G model 273A potentiostat/galvanostat (AUTOLAB, Eco Chemie.). A Pt wire and Ag/AgCl (in 3 M KCl) were used as counter and reference electrode, respectively. Working electrodes were carefully prepared as following procedures: a glassy carbon was mechanically polished with 1, 0.3, and 0.05 μm Al_2O_3 pastes until a mirror-like surface was obtained and then washed thoroughly with acetone and distilled water to remove residual alumina particles completely. The polished glassy carbon electrode was activated electrochemically in a 0.5 M sulfuric acid solution by applying a potential sweep between −0.3 and 1.3 V versus Ag/AgCl at a scan rate of 100 mV s^{-1} up to steady-state conditions [30]. 0.1 g of the catalysts was suspended in 2 ml of Millipore de-ionized water (18 MΩ cm) containing 20 ml of Nafion® ionomer solution (in 5 wt.% solution from Aldrich), in which the latter is served as an adhesive and a proton conductor. This catalyst slurry mixture was ultrasonically scattered for 20 min to prepare well-dispersed and homogeneous catalyst ink. Then 3 μl of the catalyst ink was transferred using a micropipette onto the prepared glassy carbon disk electrode surface (with geometric area of *ca.* 0.07 μl), followed by drying in an oven at 343 K for 30 min to prepare the catalyst film impregnated on the vitreous carbon disk electrode as the working electrode. Before CV measurements, the electrolyte solution of 0.5 M H_2SO_4 was purged fully with the pure N_2 in order to degas oxygen that might exist in the solution. The CVs were recorded in the range of −0.2 and 1.0 V (versus Ag/AgCl) at a scan rate of 50 mV s^{-1} in the 0.5 M H_2SO_4 in the absence or presence of 2.0 M of individual alcohols (methanol, ethanol, and 1-propanol), respectively.

3. Results

3.1. Structural change of PtSn/C with Sn content

Fig. 1 shows XRD patterns of the carbon-supported 20 wt.% Pt and PtSn catalysts with Pt:Sn ratios, in which the characteristic peaks of a crystalline face centered cubic (fcc) Pt phase from (1 1 1), (2 0 0), (2 2 0), and (3 1 1) planes appeared at the corresponding diffraction angles. The first broad peak around 25° is associated with (0 0 2) plane of the hexagonal structure of Vulcan XC-72R carbon black support [31]. It can be also seen from Fig. 1 that the typical fcc-Pt diffraction peaks in all PtSn/C catalysts appear to be broadened due to small particle size effect. There were no noticeable peaks for a pure Sn or its oxides in our XRD measurements, indicating a good degree of alloying between Pt and Sn although tin oxides phase as "X-ray amorphous" form [32] might be involved. In particular, the diffraction peaks were slightly but consistently shifted to lower 2θ values in the PtSn/C catalysts with increasing Sn content, as described in the right figure for the enlarged Pt (2 2 0) peak; such a consistent shift could be an evidence for the alloy formation between Pt and Sn caused by incorporation of Sn atoms to the fcc structure of Pt [10].

The average particle sizes and lattice parameters for the single-phase Pt and PtSn (solid solution) were evaluated using the full width at half maximum (FWHM) and the angular position ($2\theta_{max}$) of the (2 2 0) peaks [22], as summarized in Table 2. The average size of the catalyst particles was calculated from the Gaussian-fitted (2 2 0) peak according to the following Scherrer formula:

$$L = \frac{0.94\lambda_{K\alpha 1}}{B_{(2\theta)}\cos\theta_{max}},$$

where L denotes the average particle size, the value 0.94 comes from spherical crystallite geometry (cubo-octahedral shape), $\lambda_{K\alpha 1}$ is the wavelength of X-ray radiation (1.54056 nm), θ_{max} is the angular position at the (2 2 0) peak maximum, and $B_{(2\theta)}$ is the full width at half maximum (FWHM) of the peak broadening in radians. The Pt (2 2 0) diffraction peak was used as the reference so as to avoid possible disturbances from the carbon black [30]. However, in case of PtSn/C catalyst with the highest Sn content, i.e. Pt_1Sn_1/C, the typical (2 2 0) peak of the Pt-fcc structure was too broad to calculate the average particle size with the Scherrer formula, which might be attributed to a great diminishment of Pt crystalline properties by too large amount

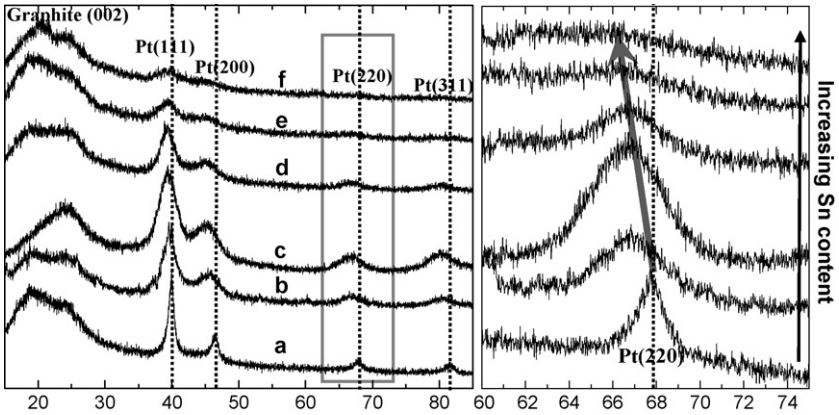

Fig. 1. X-ray diffraction patterns of the prepared 20 wt.% Pt/C and PtSn/C catalysts with different Pt:Sn atomic ratios over the scan range 10–85° and the selected scan range in the vicinity of Pt (2 2 0) reflection peak. (a) Pt/C, (b) Pt_4Sn_1/C, (c) Pt_3Sn_1/C, (d) Pt_2Sn_1/C, (e) Pt_3Sn_2/C, and (f) Pt_1Sn_1/C.

Table 2
Structural parameters of the catalysts characterized by XRD and TEM analyses

Catalysts	$2\theta_{max}$ [a] (°)	Lattice parameter [b] (Å)	Mean particle size (nm)	
			XRD [c]	TEM [d]
Pt/C	67.72	3.910	3.5	3.8 ± 0.5
Pt_4Sn_1/C	66.85	3.955	3.0	3.2 ± 0.3
Pt_3Sn_1/C	66.74	3.961	2.9	3.2 ± 0.3
Pt_2Sn_1/C	66.67	3.965	2.5	2.2 ± 0.2
Pt_3Sn_2/C	66.32	3.983	2.4	2.3 ± 0.2
Pt_1Sn_1/C	66.08	3.996	–	2.7 ± 0.3

[a] The angular position of Pt(2 2 0) reflection peak.
[b] Lattice parameter calculated from XRD measurement.
[c] Mean particle diameter of the metal catalyst calculated by line broadening of powder XRD peak at around 67° using the Scherrer equation.
[d] Mean particle diameter of the metal catalyst from TEM images using at least 100 visible particles.

of Sn incorporation. The lattice parameter changes of the PtSn/C catalysts, reflecting the formation and degree of alloying [30], are also given in Table 2. While the lattice parameter of 3.91 Å for the Pt/C catalyst is in a good agreement with that of nanosized Pt particle reported in elsewhere [18,31], the crystalline lattice parameters for all the PtSn/C catalysts are greater than that of Pt/C catalyst and appear to increase slightly with increasing Sn content, indicating the lattice dilation as Sn atoms are incorporated to the fcc lattice of Pt crystallites. Such an extended lattice parameter on the PtSn/C catalysts appears to increase linearly with Sn content as demonstrated in Fig. 2 for our catalyst samples, which is in line with the Vegard's law relation [32].

Fig. 3 depicts representative TEM images of the carbon-supported Pt and PtSn catalysts with different Pt:Sn atomic ratios. High resolution image as included in the inset image of Pt_3Sn_1/C reveals that the catalyst nanoparticles are crystalline with an asymmetric facetted cubo-octahedral shape. All the PtSn/C catalysts have the similar metal particle sizes of 2.8 ± 0.4 nm regardless of Sn content, which were estimated

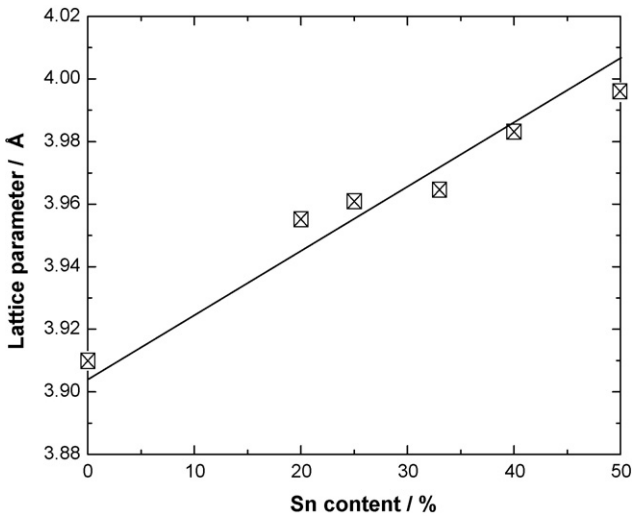

Fig. 2. The change of the lattice parameter of the PtSn catalysts with the amount of Sn incorporated.

by averaging the diameter of at least 100 different nanoparticles seen in the TEM images. Although the particle sizes from TEM seem to be relatively larger than those from XRD in our study because the crystallite size calculated from XRD results might be closely associated with the area of coherent diffraction, both the XRD and TEM results jointly indicate that all synthesized catalysts in this work are highly dispersed on the carbon support, demonstrating borohydride reduction method with freeze-drying procedure could provide a convenient, inexpensive and suitable method to prepare nanosized catalysts. There appeared no significant change in the metal particle size with variation of Sn content under our preparation condition, allowing particle size effect to be excluded from influential parameters for the electrocatalytic activity over the carbon-supported PtSn catalysts.

Fig. 4 shows Fourier transformed (FT) EXAFS profiles of the Pt/C and PtSn/C catalysts together with the Pt foil reference for the Pt–Pt bond. These FT-EXAFS data are characterized by a main peak located at a radial distance of 2.75 Å, which is likely due to the phase-uncorrected first shell of Pt–Pt interaction [15,33] for the single component of Pt/C and the interfered interaction with Pt–Sn bonds for the alloyed PtSn/C systems. It should be noted that the radial bond distances of Pt–Pt bond and Pt–Sn bond are too close to be separated in the radial distance function (RDF) spectra [15,34]. In order to obtain quantitative information for the coordination number (CN) and radial distance of the local environment of Pt, we fitted the experimentally-derived RSF with theoretically-synthesized Pt–Pt and Pt–Sn scatterings, as summarized in Table 3. The CN of the Pt/C catalyst showed about 8.6, which is definitely smaller than the theoretical CN value 12 of the fcc crystallite like Pt foil because of its nanosize feature as estimated to be *ca.* 3.8 nm of the particle diameter from the TEM. For the alloyed PtSn catalysts, the total CNs including both Pt–Pt and Pt–Sn interaction were in the range of 7.2–8.1, of which might be correlated with the TEM observations that the average particle sizes were in nanosizes of 2–3 nm (Table 2). However, considering the particle sizes of the PtSn/C catalysts, the CNs obtained from the EXAFS fitting would be underestimated by 1–2 because they would be 8–10 from the average particle sizes measured from TEM of our PtSn catalyst systems when the CN are simulated with respect to the diameter of cubo-octahedron nanoparticles according to the literature [35].

3.2. Electronic change of PtSn/C with Sn content

Fig. 5 shows XPS spectra of Pt 4f and Sn 3d for the carbon-supported Pt and PtSn catalysts with variation of Sn content. The Pt 4f XPS spectra contain two peaks corresponding to Pt $4f_{7/2}$ and $4f_{5/2}$ states from the spin-orbital splitting and each peak was deconvoluted with two different Pt oxidation states of Pt(0) and Pt(II) in order to identify the higher oxidation states of Pt. The Pt $4f_{7/2}$ peak around 71 eV corresponds to zero-valent Pt, while the Pt $4f_{7/2}$ peaks around 72 eV could be assigned to Pt^{2+} states as PtO or $Pt(OH)_2$ due to surface layer formation of $Pt–O_{ad}$ bonds [35–39]. The fraction of two Pt species (Pt^0 and

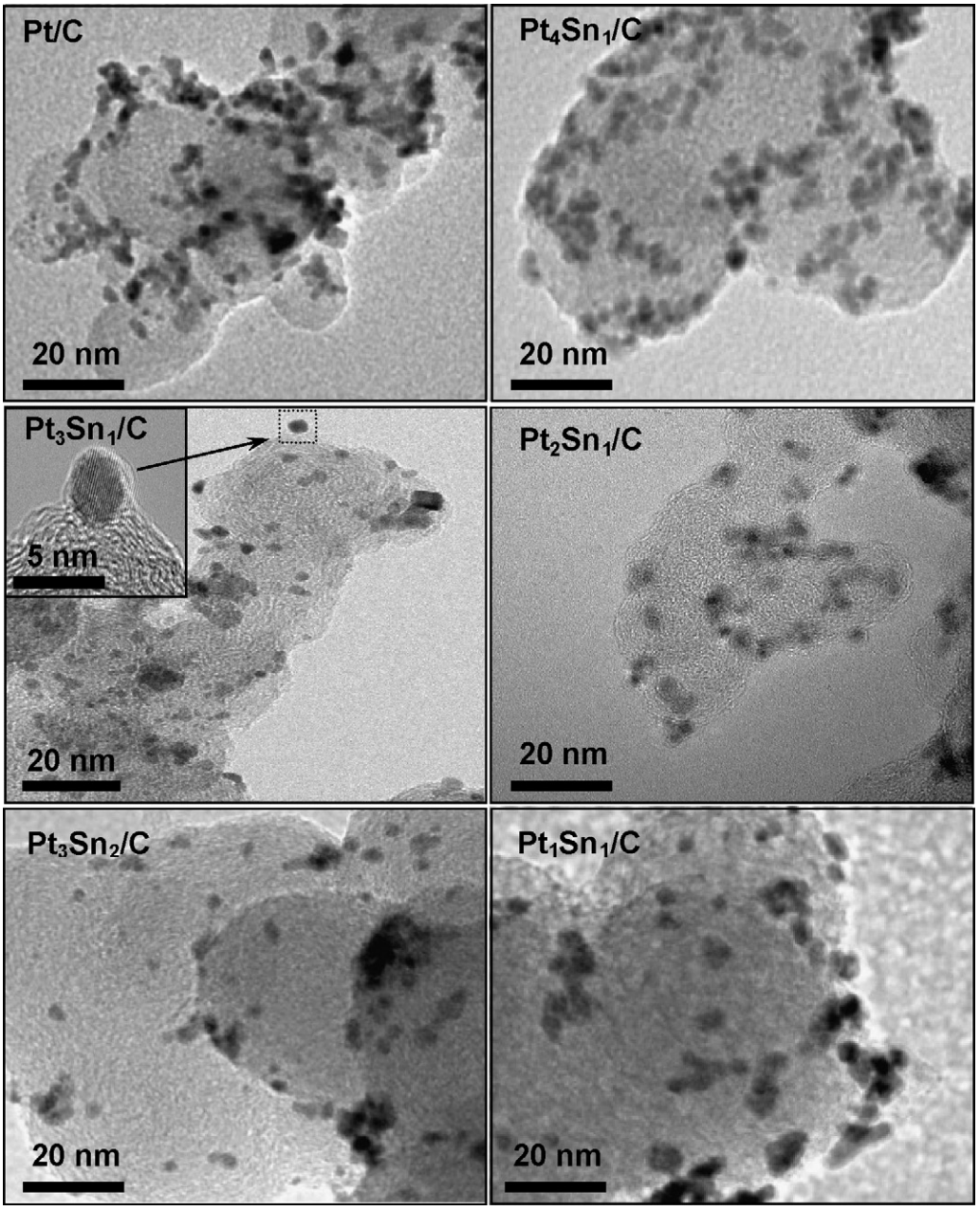

Fig. 3. Representative TEM images of the 20 wt.% carbon-supported Pt and PtSn catalysts with different Pt:Sn ratios.

Pt^{2+}) could be estimated from relative intensities of their deconvoluted peaks, as summarized in Table 4. It is found that Pt^0 is a predominant species (65–75%) in all PtSn/C catalysts with small amounts of the oxidized Pt species (25–30%) that might be produced on the catalyst surface through passivation process during the sample preparation. It is noteworthy that the binding energy shift to lower energies by 0.3–1.0 eV appeared in all PtSn/C catalysts compared to the Pt/C catalyst, which may be caused by electronegativity differences in the elemental Pt and Sn, leading to charge transfer from the less-electronegative Sn to the more-electronegative Pt. For Sn 3d XPS spectra in Fig. 5 we have observed that XPS–responsive surface state of Sn is oxidic (e.g., SnO, SnO_2, or Sn hydroxides) [35,38] independent of the amount of Sn content in the PtSn/C catalysts. Discrimination between Sn(II) and Sn(IV) species from the XPS results was not possible due to a very small difference in the binding energy of both species. However, judging from the width and shape of XPS peak we could infer that only one chemical state of Sn might be involved in the PtSn catalyst systems, which would be produced due to strong affinity of tin toward oxygen species (oxophilicity), thereby being easily oxidized by dioxygen and/or H_2O from the atmosphere.

To elucidate composition change of Pt and Sn atoms, the surface Sn/Pt atomic ratios calculated from the XPS signal were plotted versus the bulk Sn/Pt atomic ratios measured from ICP-AES, as shown in Fig. 6. It appears that the surface atomic ratios were almost same as those of the bulk compositions until the

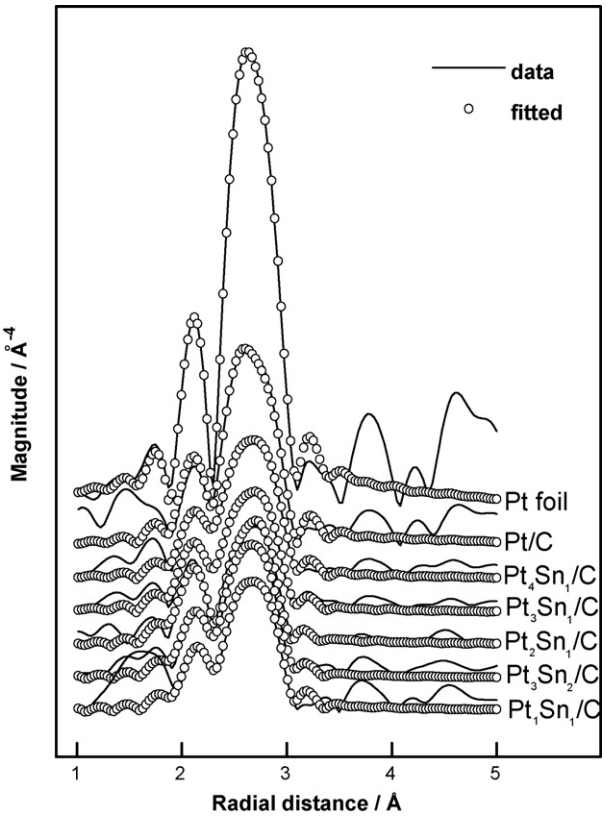

Fig. 4. FT-EXAFS profiles for the Pt foil, Pt/C, and a series of PtSn/C catalysts with sample spectra (–) and the fitted functions (○).

Sn/Pt = 1, but significantly differed for the higher Sn/Pt ratios as seen by the deviated data from the theoretical line in 45° slope, which implies a heterogeneous nature of the composition profile for Sn and Pt in the Sn-rich PtSn catalysts. Noticeably, the surface Sn/Pt atomic ratios tend to be higher than the bulk values, indicating that the PtSn/C catalysts may cause significant surface Sn enrichment by segregation of Sn onto the surface especially in the samples with higher Sn content. This behavior may be explained by thermodynamics that the nature of Sn element which has a lower surface free energy than platinum causes migration of Sn from bulk to surface, like same results observed for silica-supported bimetallic PtSn catalysts by several groups [40,41]. Therefore, from the observations that the Pt:Sn ratio showed the greater Sn/Pt ratio values measured from the surface-specific XPS technique than those quantified with the ICP for the bulk compositions (Table 1) and that the more Sn enrichment happened preferentially on the surface with Sn addition by comparing the surface Sn/Pt versus bulk Sn/Pt ratios (Table 4 and Fig. 6), these compositional analyses unambiguously indicate that the structures of PtSn particles in this study consist of Sn-rich surface layer and Pt-rich inner part.

Fig. 7 represents the Pt L_3 edge XANES spectra obtained for 20 wt.% Pt/C and PtSn/C catalysts with different Pt:Sn atomic ratios. The absorption at the Pt L_3 edge (11564 eV) corresponds to $2p_{3/2} \rightarrow 5d$ electronic transitions [15,41]. The entire XANES shapes for the PtSn/C are similar to those of the Pt foil and Pt/C except the peak intensity after the edge absorption. The strong peak above the edge energy position at the dashed vertical line is closely associated with density of vacant 5d electronic states in Pt [41], which is called the white line peak and frequently recognized as an important parameter in catalytic activity [15]. The white line magnitudes were smaller in all PtSn/C catalysts than that of Pt/C catalyst and showed a decreasing propensity with increasing Sn content up to Pt/Sn ratio of 2, which can be attributed to partial filling of the unoccupied Pt 5d orbital by electrons that are donated by adjacent Sn, thus the electronic transition of $2p \rightarrow 5d$ is suppressed along with the result of smaller white line intensities. It may be correlated with the EXAFS results that Pt–Sn bond distance seemed to slightly decrease with increasing Sn amount up to Pt/Sn ratio of 2 via a stronger interaction between the Pt and added Sn, although the WL intensities appeared to increase a little again for the highest Sn added catalysts such as Pt_3Sn_2/C and Pt_1Sn_1/C but still smaller than that of Pt/C, in which the latter may be attributed to the preferential Sn-rich layer formation as mentioned earlier. These analyses of electronic structures with XANES were included in Table 4 for the quantitative white line values with the edge energy analysis.

3.3. Electrocatalytic activities of PtSn/C with Sn content

The catalytic activity of the Pt and PtSn/C catalysts were examined by cyclic voltammetry (CV) technique for the

Table 3
EXAFS fitting results for the first shell of Pt/C and PtSn/C catalysts with Sn contents

Catalyst	Pt–Pt interaction		Pt–Sn interaction		ΔE^c (±1 eV)	$\sigma^2 \times 10^{-3d}$ (±0.001 Å^2)	R factor ($\times 10^{-3}$)
	N^a (±1)	R^b (±0.01 Å)	N (±0.1)	R (±0.01 Å)			
Foil	12	2.76	–	–	4.77	4.9	0.6
Pt/C	8.63	2.76	–	–	5.06	7.1	2.1
Pt_4Sn_1/C	7.19	2.77	0.88	2.77	3.86	7.8	1.0
Pt_3Sn_1/C	6.81	2.76	0.78	2.72	1.87	7.8	1.3
Pt_2Sn_1/C	6.34	2.75	0.90	2.68	−0.10	7.2	2.8
Pt_3Sn_2/C	6.73	2.76	0.57	2.73	2.04	7.3	1.0
Pt_1Sn_1/C	6.23	2.76	0.68	2.74	5.04	7.3	1.1

[a] The average coordination number for the coordination shell.
[b] Inter-atomic distance.
[c] E_0 shift of the path.
[d] Debye–Waller factor.

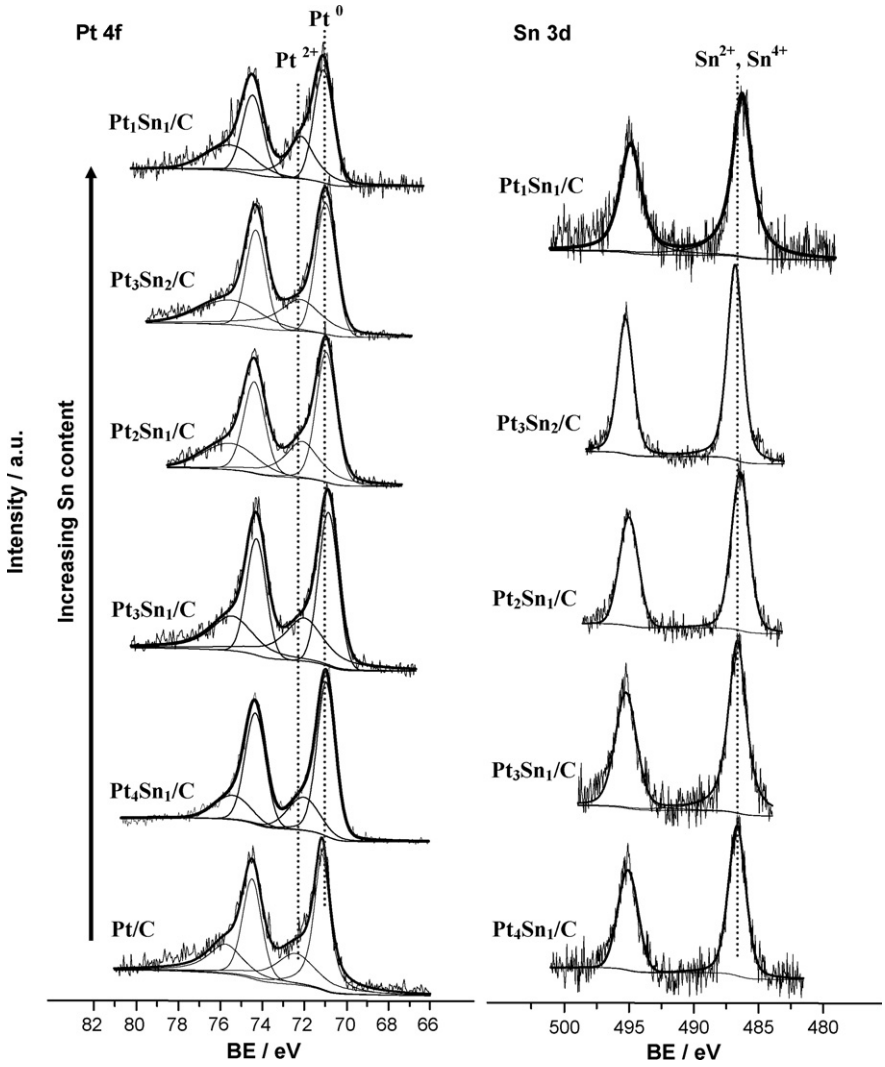

Fig. 5. X-ray photoelectron spectra of Pt 4f and Sn 3d for the Pt/C and various PtSn/C catalysts.

Table 4
Electronic parameters of the catalysts characterized by XPS and XANES analyses

Catalyst	Binding energy (eV)		Sn/Pt[a] (atomic ratio)	XANES parameters	
	Pt $4f_{7/2}$	Sn $3d_{5/2}$		E_0 (eV)	WL intensity (a.u.)
Pt foil	–	–	–	11564.0	1.25
Pt/C	71.2 (72)[b] 72.4 (28)[b]	–	–	11564.0	1.64
Pt_4Sn_1/C	70.1 (74) 72.0 (26)	487.1 (100)	0.38	11563.8	1.29
Pt_3Sn_1/C	70.9 (70) 72.0 (30)	487.1 (100)	0.68	11563.9	1.25
Pt_2Sn_1/C	70.1 (71) 72.1 (29)	486.9 (100)	0.93	11564.0	1.19
Pt_3Sn_2/C	70.1 (72) 72.2 (28)	487.3 (100)	1.82	11563.9	1.30
Pt_1Sn_1/C	71.0 (64) 72.1 (36)	487.0 (100)	2.00	11564.0	1.43

[a] Surface Sn/Pt atomic ratio calculated from XPS by using peak areas normalized on the basis of sensitivity factors [22].
[b] Relative % of the Pt^0 and Pt^{2+} species.

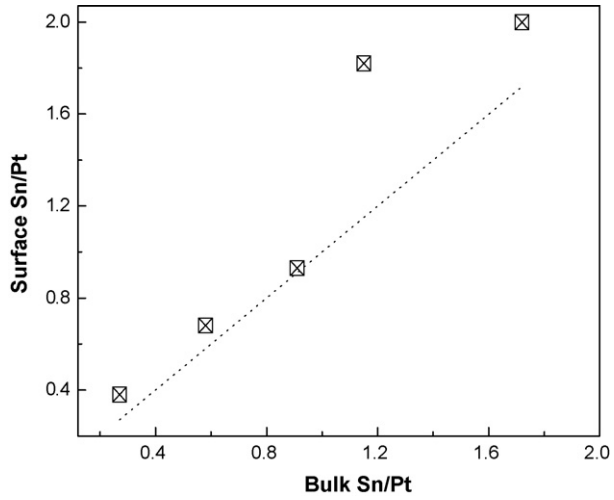

Fig. 6. Sn/Pt atomic ratios on the surface calculated by XPS analysis with increasing Sn/Pt atomic ratios obtained by ICP.

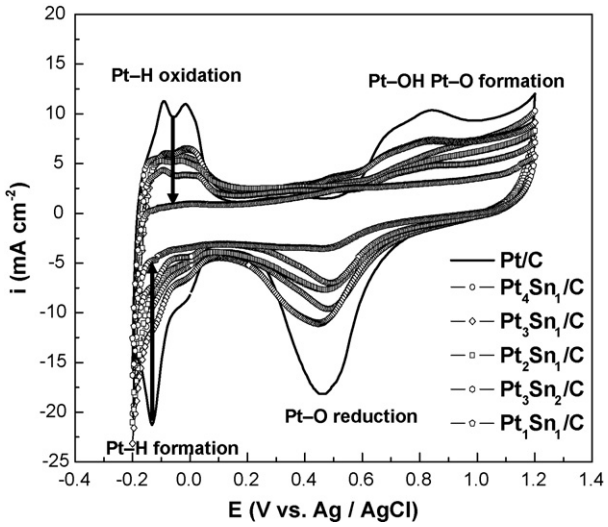

Fig. 8. Cyclic voltammograms of the Pt/C and PtSn/C catalysts with variation of Sn content in 0.5 M H_2SO_4 electrolyte at a scan rate of 50 mV s^{-1} at room temperature. Current densities were normalized by geometric area of the working electrode (*ca.* 0.07 cm^2).

electrooxidation reactions of methanol, ethanol, and 1-propanol, respectively. Prior to the alcohol oxidation, CV tests of the carbon-supported catalysts were first studied in a supporting electrolyte of acid solution (in the absence of alcohol) in order to characterize interactions of the metal surface with hydrogen and establish potential range for the electrochemical stability of these materials. Fig. 8 shows typical CV curves of the Pt/C and PtSn/C catalysts in a 0.5 M H_2SO_4 electrolyte at room temperature, which were obtained using a half cell system at a scan rate of 50 mV s^{-1} in the potential range of −0.2 to 1.2 V (versus Ag/AgCl). Since the same amount of metal loading (*ca.* 0.024 mg with ±5% error) was mounted on the working electrode for all tests, the currents normalized by geometric area of the working electrode (i.e., current density) directly correspond to specific activities based on the mass of metal. The voltammograms of Pt/C catalyst after the 10th cycle were identical and reproducible without any appreciable changes in all experiments, by showing well-defined adsorption and desorption peaks of hydrogen in potential range of −0.2∼0.1 V (versus Ag/AgCl) over the fcc-Pt with different crystalline facets [42], where the influence of anions in the electrolyte was assumed to be negligible for the hydrogen adsorption–desorption in our experimental condition. In case of the PtSn/C catalysts, all CVs showed similar features to that of Pt/C (the solid line), but exhibited differences in hydrogen region by showing broad and smaller hydrogen adsorption–desorption peaks instead of the well-defined hydrogen characteristics for the polycrystalline Pt as the Pt/C, which might be caused by structural modifications of Pt due to the Pt–Sn interaction.

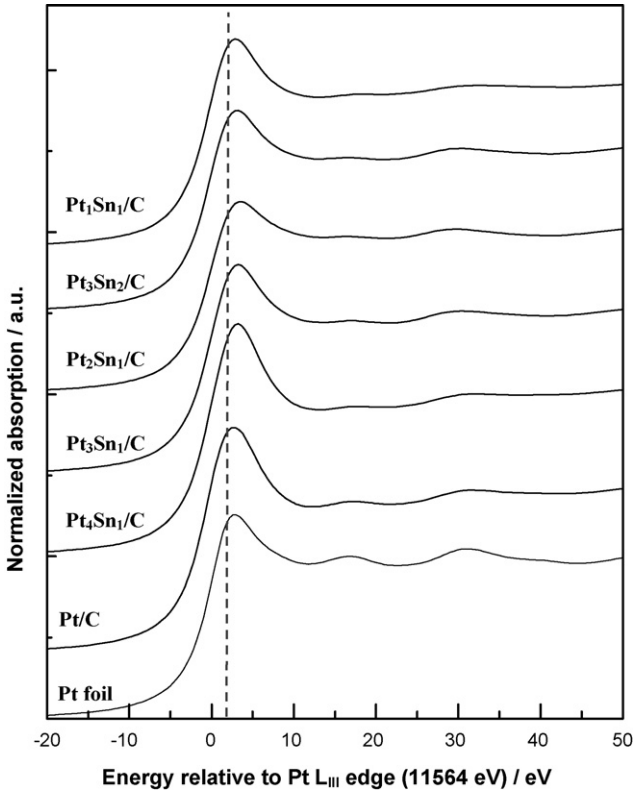

Fig. 7. Pt L3 edge XANES spectra for the Pt/C and PtSn/C catalysts together with Pt foil as a reference.

The coulombic charge for hydrogen oxidation obtained after subtracting charge contributed from the double layer region was used to estimate electrochemical active surface (EAS) areas with assumptions that the normalized charge density for a monolayer of adsorbed hydrogen on polycrystalline platinum is 210 μC cm^{-2} [15] and all platinum mounted on the working electrode is considered electrochemically active. Table 5 summarizes the EAS values with the Sn content, which was obtained using the hydrogen desorption areas in the Pt–H oxidation region. The hydrogen desorption area unequivocally depends on the quantity of platinum loading, thereby resulting in decrease of EAS with the increase of Sn content as listed in the Table 5. Note again that we loaded almost same amount of metal (Pt + Sn) on the working electrode; i.e. the less amount of Pt was indeed used for the PtSn/C catalysts with increasing Sn

Table 5
The quantitative analysis of the cyclic voltammograms for the Pt/C and PtSn/C catalysts in the absence and the presence of 2.0 M of alcohols

Catalysts	Desorption area[a] (cm^2)	EAS ($m^2\ g_{-Pt}^{-1}$)	Forward peak current density ($mA\ cm^{-2}$)		
			MeOH	EtOH	1-PrOH
Pt/C	21.1	87.7	56	50	14
Pt_4Sn_1/C	18.8	97.9	82	141	33
Pt_3Sn_1/C	18.4	102.6	140	143	35
Pt_2Sn_1/C	17.8	111.4	102	172	56
Pt_3Sn_2/C	13.1	91.1	69	103	87
Pt_1Sn_1/C	4.8	39.9	64	73	28

[a] Calculated hydrogen desorption area by taking 210 $\mu C\ cm^{-2}$ [15] as the electrical charge for a monolayer of hydrogen in a smooth Pt(1 0 0) electrode.

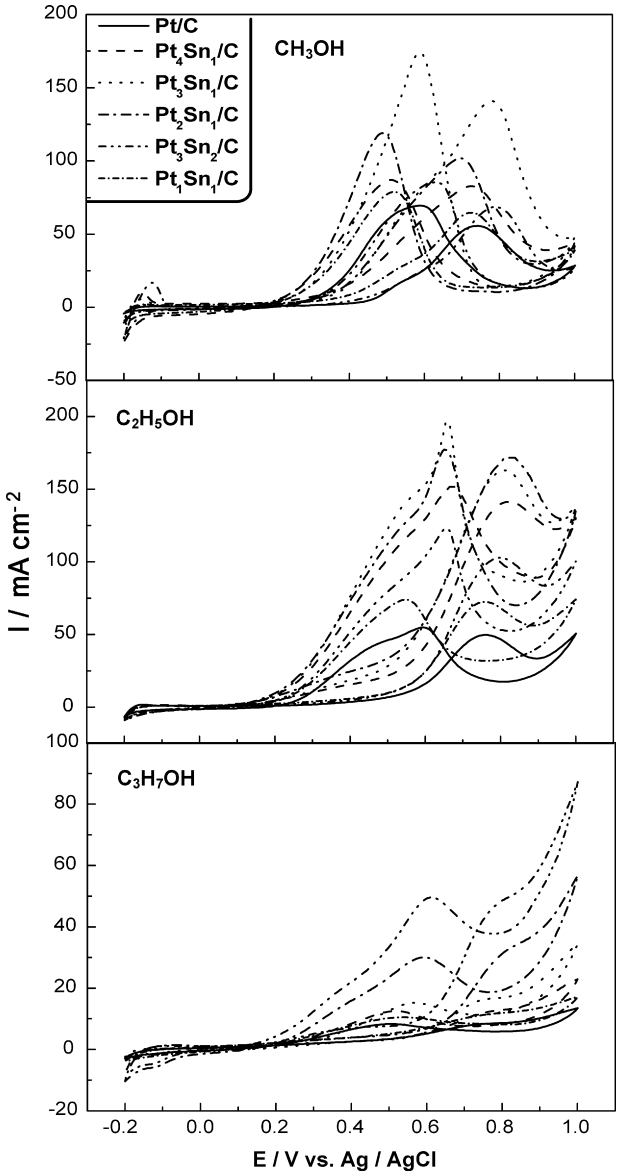

Fig. 9. CVs of the Pt/C and PtSn/C catalysts in 0.5 M H_2SO_4 with 2 M CH_3OH, C_2H_5OH, and C_3H_7OH at a scan rate of 50 mV s^{-1} at room temperature, respectively.

content. Interestingly, the EAS normalized by gram of Pt seems to be influenced with Sn/Pt atomic ratios in that initial increase of the EAS value was observed with increasing Sn content up to Pt:Sn of 2:1, then the EAS tends to drop with further Sn added, and a dramatic decline to *ca.* 40 m^2 g Pt^{-1} is observed for the highest Sn-containing Pt_1Sn_1/C catalyst in our study.

Although platinum itself is generally known as one of the best catalyst for the electrooxidation of alcohols, especially in the acid environment [21], it alone has limited ability for C–C bond cleavage and CO oxidation, which are often realized as the rate-determining steps in the electrooxidation of alcohols. Therefore, modifications of the Pt electronically and/or structurally with second metal would be largely effective toward alcohols electrooxidation as shown in Fig. 9 of CV curves over the PtSn/C catalysts. The scan potential was from −0.2 to 1.0 V (versus Ag/AgCl) at a scan rate of 50 mV s^{-1} and the 10th cycle from all CV curves was selected in order for reproducible and reliable electrocatalytic performance in the half cell reaction. The shapes of curves are typical for the electrooxidation reactions of simple organic alcohols, showing two anodic current peaks in positive and negative sweeps, respectively; they are related to oxidation reactions of alcohol in the positive sweep and of incompletely oxidized carbonaceous residues on the catalyst surface during the negative sweep. The latter intermediates are likely to be strongly adsorbed on the Pt surface, blocking the effective and active catalyst sites for next turnover, thus making the anodic reactions more sluggish. It was also observed that hydrogen interaction peaks were reduced as compared with that obtained from the absence of alcohol (see Fig. 8) because alcohol and/or their intermediates can occupy the catalyst active sites, thus inhibiting the adsorption of hydrogen [29]. By comparing the characteristics of the CVs as summarized in Table 5, addition of Sn into Pt leads to substantial enhancements in the catalytic activity for the electrooxidation of alcohols tested here. The peak current densities are improved for methanol, ethanol, and 1-propanol, respectively, over all PtSn/C catalysts compared to the Pt/C catalyst, suggesting additions of Sn into Pt can significantly improve the reaction rate regardless of the Sn contents up to 50%. Interestingly, the activity enhancements with the addition of Sn become much larger in this work by 2.5 , 3.5 , and 6.0 folds, when we consider the best composition of Pt and Sn to give maximum activity like Pt_3Sn_1/C, Pt_2Sn_1/C, and Pt_3Sn_2/C for methanol, ethanol, and 1-propanol, respectively. Also it can be easily expected that these activity improvements should be greater in terms of mass activity (i.e., mA mg_{Pt}^{-1}) because the actual Pt loadings were less used in the PtSn series than the Pt alone case.

4. Discussion

4.1. Bimetallic PtSn catalysts

Bimetallic PtSn catalysts supported over carbon, alumina, and silica had been widely used for reforming and refining processes to obtain higher activity, selectivity, and improved stability. It has been established that promoting effects of Sn in

Pt catalysts and mechanism of Sn incorporation can depend on pretreatment of support, catalyst preparation, and Sn/Pt ratio [43–53]. The effects of Sn on Pt catalysts have been believed to be associated with modification of geometric and electronic structures by Pt–Sn interactions, thus consequently leading to changes in catalytic activities. Recently, the bimetallic PtSn supported on carbon have been recognized again and studied in PEM type fuel cells as the improved electrode material for CO tolerance and alcohols oxidation [5,16–19].

For the aspect of geometric structure modification on the PtSn/C catalyst, the XRD (see Fig. 1 and Table 2) and EXAFS (see Fig. 4 and Table 3) analyses jointly indicated that the geometric environment was changed with Sn addition to the fcc Pt crystallites by forming solid solution of PtSn alloy phase, accompanying an expansion of lattice parameter. This elongation of bonding structure may affect catalytic reaction pathways that require specific geometric arrangements of the surface atoms, thus leading to change of catalytic properties. According to DFT calculations by Alcalá et al. [54], surface transition species derived from ethanol on a Pt (1 1 1) plane for cleavage of C–C and C–O bonds may be sensitive to geometric parameters, i.e. bond lengths and angles. It has been also reported by several authors [18,55,56] that the extended lattice parameter of the Pt may facilitate the C–C cleavage, thus improve their catalytic activity for the electrooxidation of alcohols. It would be noted that the EXAFS fitting results for the local structural information such as coordination numbers and bonding distances in our study might not reflect such systematic changes in the geometric parameters of the PtSn systems as observed from XRD. The apparent discrepancy on the structural analyses between XRD and EXAFS and such weak trends in the fitting results might come from the preferential Sn enrichment on the surface with Sn addition.

When it comes to electronic structure modification of the bimetallic PtSn system, the most noticeable change would be the charge transfer from Sn atoms to neighboring Pt atoms. We observed the decreases of Pt 4f binding energy in XPS (see Fig. 5 and Table 4) and white line intensities in XANES (see Fig. 7 and Table 4) of PtSn/C catalysts with respect to the Pt/C catalyst, which can be attributed to charge transfer from Sn to Pt [17]. In particular, it is known that a Sn atom has four valence electrons available to modify Pt even with a small amount of Sn incorporation [57]. This electronic modification in unfilled d band states of Pt atoms may cause a weaker bond between carbon atoms and surface Pt atoms, thus reducing or preventing catalytic poisoning. On the other hands, the adsorption ability of Pt catalyst with other molecules such as hydrogen and alcohols might be simultaneously diminished, but whose negative effect would compromise the beneficial effect of the poison-tolerance during the electrooxidation processes. As a chemical consequence of Pt and Sn, whereas oxidic impurities of surface Pt sites are partially decreased as Pt sites tend to be reduced as the surface Sn sites are readily oxidized to form tin oxide species, which was agreed with XPS results (Fig. 5 and Table 4). These ''labile-bonded'' oxygen-containing species on the Sn surface may facilitate the electrooxidation of adsorbed carbonaceous residues to CO_2 [58]. Therefore, the Sn addition modifies the electronic environment of PtSn catalysts by influencing the electron affinities of the surface Pt atoms and produces surface oxygenated species which can act as an oxidant source, thereby increasing stability through efficient oxidation of surface poisoning species [44].

4.2. Effects of Sn content in the PtSn on the electrocatalytic activity

4.2.1. Hydrogen electrooxidation

EAS values for hydrogen oxidation calculated from the CVs in Fig. 8 were summarized in Table 5 with respect to the nominal Sn/Pt atomic ratios, in which the EAS values appeared to be strongly dependent on the Sn/Pt atomic ratios by showing a volcano type curve. When Sn was added up to *ca.* 33 wt.% (the nominal Pt:Sn = 2:1), the EAS values were monotonically increased from 87.7 $m^2\,g\,Pt^{-1}$ for the Pt/C catalyst to 111.4 $m^2\,g\,Pt^{-1}$ for the Pt_2Sn_1/C catalyst. One possible explanation of this increase is that the slightly extended bonding distances in the local structure of Pt might promote the hydrogen oxidation with Sn addition up to the Sn/Pt ratio along with the electronic modification from the charge transfer from Sn to Pt. As far as the geometric modification is concerned on the interaction of hydrogen and Pt, it is known that the dissociative chemisorption of hydrogen molecule on Pt at room temperature requires adjacent vacant Pt surface sites, as Balakrishnan et al. [59] found a strong Sn/Pt ratio dependence of hydrogen gas uptake in bimetallic PtSn/Al_2O_3 catalysts. However, in case of the Pt_1Sn_1/C catalyst with the highest Sn content in our study, the EAS values steeply fell to about the half and one-third of those of monometallic Pt/C and bimetallic Pt_2Sn_1/C catalysts, respectively; this EAS reduction by addition of too much Sn could be interpreted in terms that the drastic reduction of Pt ensemble sites for the hydrogen reaction is likely to be expected due to the dominant occupation of Sn into the Pt sites and the electrical conductivity of the PtSn nanoparticles may be decreased by forming larger amounts of Sn-rich phase on the catalyst surface.

4.2.2. Alcohol electrooxidation

Simple C_1 compounds (e.g., methanol and formic acid) and C_2 or higher alcohols (e.g., ethanol, ethylene glycol, propanol, and butanol) have been studied as fuels for DAFC at low temperatures. While methanol electrochemistry has been well established by extensive studies [21,47,60,61], the electrochemical oxidations of the alcohols that possess several carbon atoms are still under discussion because of much complicated reaction mechanism. Fig. 10 illustrates possible reaction pathways (a) and schematic surface reactions (b) over the bimetallic PtSn-supported carbon catalysts with successive donation of electrons that may be involved in the electooxidations of the C_1–C_3 alcohols as denoted as $C_nH_{2n+1}OH$ for convenience. Alcohols undergo adsorption and dehydrogenation steps on the active Pt sites to give adsorbed reaction intermediates before the cleavage of C–C and C–O bond, while the dissociative adsorption of water is believed to occur on the Sn sites to form surface oxygen-containing species, in which

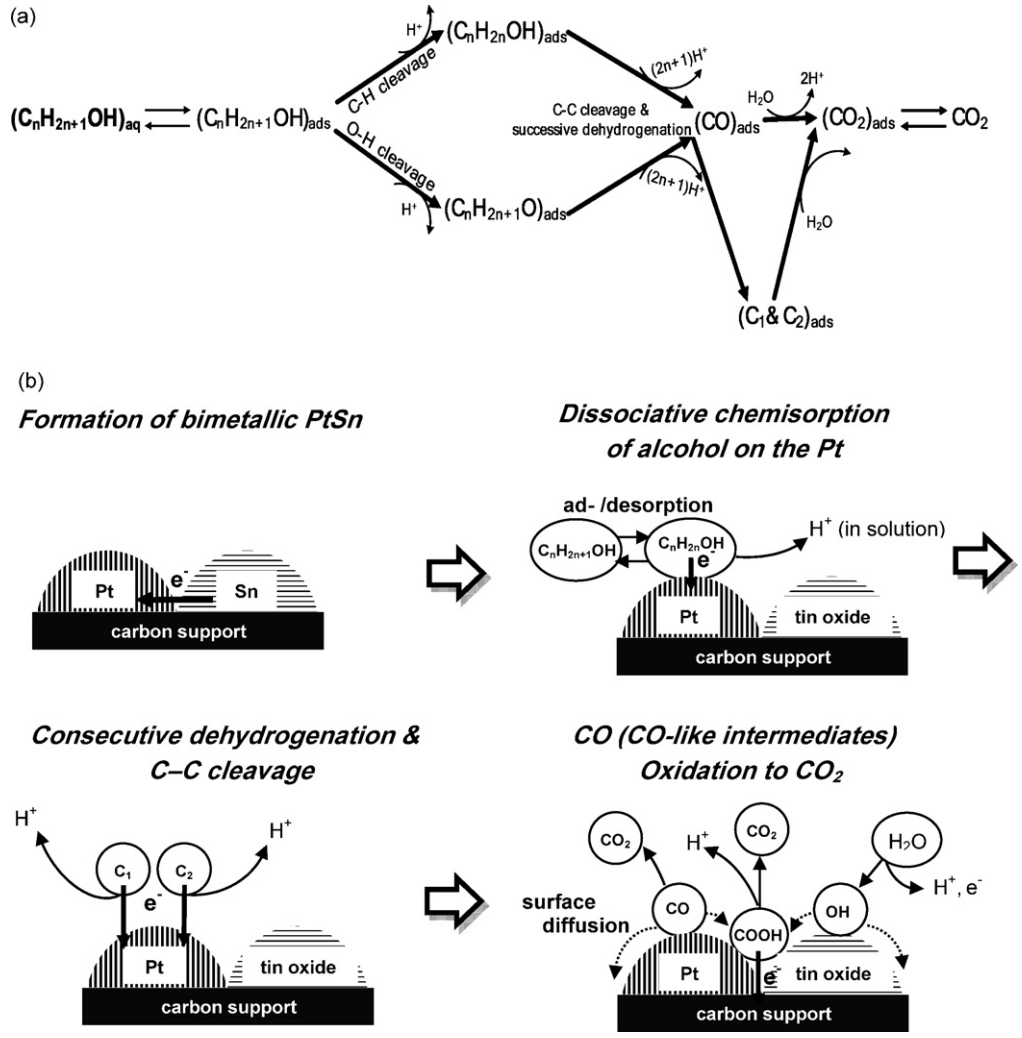

Fig. 10. Possible reaction pathways (a) and illustration of schematic surface reactions (b) over the bimetallic PtSn catalyst for the electooxidations of the C_1–C_3 alcohols as denoted as $C_nH_{2n+1}OH$.

the latter are expected to be able to facilitate the oxidative removal of the intermediate residues. Zhou et al. reported that Sn surface sites are assumedly free to supply adsorbed OH species as CO does not prefer to bind with Sn surface sites. Obviously, Sn is able to form oxygen-containing species at lower potential than Pt that help to activate CO (or CO-like intermediates) oxidation [55]. The surface reaction is the C–C cleavage with consecutive dehydrogenation process which is one of the critical steps in alcohol electrooxidation by determining overall reaction rate and efficiency [55]. As a result of the C–C cleavage with several surface-catalyzed electrochemical reactions, C_1 and C_2-type intermediates species are left on the surface, poisoning the Pt catalyst. The subsequent reaction is surface reaction between CO (or C_1 and C_2-type intermediates) and OH (or oxygenated species) on the catalyst surface such as CO oxidation, i.e., $CO_{ads} + OH_{ads} \rightarrow CO_2 + H^+ + e^-$.

Fig. 11 plots the electrocatalytic activities obtained from the forward peak current density in the CVs (in Fig. 9) as the function of Sn/Pt atomic ratios, where each alcohol tested here presents volcano-type curve. This activity profile with Sn content has been frequently reported elsewhere, for example the References [5,43,62], however, most were dealt with individual alcohol such as methanol and ethanol, not covering the full influence of both structural and electronic features of the PtSn catalysts toward electrocatalytic activities over C_1, C_2, and C_3 alcohols. The catalysts with low Sn content showed low activities and but they were increased as the Sn content was increased up to the optimum Sn contents (*ca.* 25 wt.% for methanol, 33 wt.% for ethanol, and 40 wt.% for 1-propanol, respectively). Further Sn increases, however, caused the current densities to decline. These features may be rationalized as follows: (1) At low Sn content, there may be insufficient Sn sites to provide surface oxygen-derivatives capable of helping oxidize the adsorbed reaction intermediates. (2) Around optimum Sn content, a suitable modification might be satisfied in terms of the electronic and geometric structures for the corresponding alcohol oxidation, which can provide pertinent dilation of lattice parameter capable of assisting the cleavage of C–C bond and enough surface oxygen-containing species to oxidize carbonaceous species adsorbed on the Pt sites. With the increase of Sn content, however, it may simultaneously cause

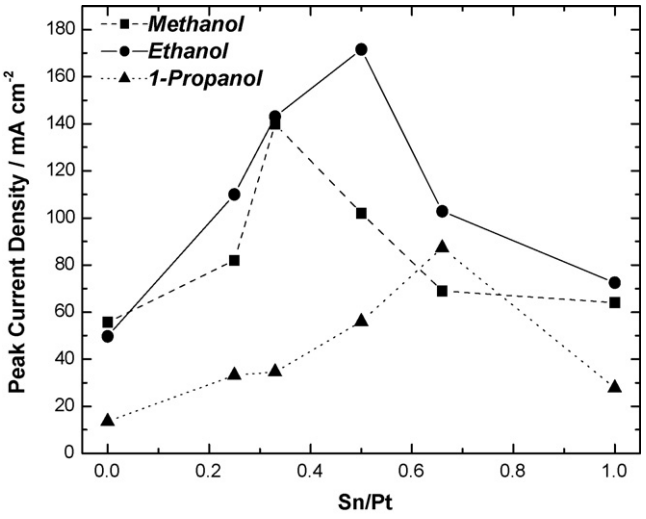

Fig. 11. The electrocatalytic activity as a function of Sn/Pt ratios for the C_1, C_2, and C_3 alcohols.

some negative effects by decreasing Pt ensembles working as active sites and/or by decreasing bond strength between Pt atoms and alcohols. These compromising effects might be balanced at the different optimum compositions for the different alcohols. (3) Too higher Sn content may seriously inhibit the dissociative chemisorption of alcohol due to too much diminished Pt ensembles size and a substantial reduction of available surface Pt active sites by larger amounts of tin species.

It is more interesting to note that the optimum Pt:Sn composition showing the maximum activity appears to consistently shift to the right direction in the Sn/Pt ratios, i.e. more Sn content is required in the order of methanol, ethanol, and 1-propanol. It has been known that the molecular structure of alcohols has a great influence on their electrocatalytic activity, especially on Pt-based catalysts. Lamy et al. [12] found that the electrooxiation rate on the single metallic platinum catalyst depends greatly on the molecular structure of primary alcohols, showing different peak current density and peak potential according to the number of carbon atoms and functional group. The higher alcohols which possess several carbon atoms make the reaction complicated considerably, where incomplete oxidation and more complex reaction are involved. Also, the increasing number of carbon atoms tends to decrease the activity due to the challenge of the C–C bond cleavage with various reaction intermediates which need further activation energies to oxidize completely. Therefore, the main point is how to make activation energies of these steps lower or oxidize them effectively. As a consequence of the increased Sn content, the increased lattice parameter might be *structurally* favorable to catalyze C–C bond breaking and increasing amounts of surface oxygen-containing species may facilitate to oxidize CO (or CO-like intermediates), and a weaker bond between Pt atoms and adsorbed carbon atoms can cause a prevention or reduction of catalytic poisoning *electronically*, which are main advantages of these bimetallic PtSn catalyst. Consequently, a compromising balance between the structural and electronic properties with variation of Sn content may be decisive factors to control their catalytic properties and electroactivities over the different alcohols.

5. Conclusions

In this study we have shown that the addition of Sn to Pt catalyst promotes the electrocatalytic activities for the different C_1, C_2, and C_3 alcohols and the optimum Pt:Sn composition showing the maximum activity was consistently shifted to the more Sn content direction in the order of more carbon-containing alcohols such as methanol (C_1), ethanol (C_2), and 1-propanol (C_3). As a consequence of the increased Sn content, the modification of structural and electronic features were observed in that the increased lattice parameter might activate C–C cleavage and the increased amount of surface oxygen-containing species facilitate to oxidize CO-like species *structurally*, and the charge transfer from Sn to Pt might cause a prevention or reduction of catalytic poisoning by partially filling of the Pt d-band vacancies *electronically*. The strong Sn/Pt atomic ratio dependence of hydrogen and alcohols electrooxiation in the bimetallic PtSn/C catalysts was observed by showing volcano-type behaviors with variation of Sn content.

Acknowledgements

This work was supported by the Korea Research Foundation (KRF-2005-205-D00023) and New & Renewable Energy R&D program (2005-N-FC03-P-01-0-001) under the Korea Ministry of Commerce, Industry and Energy (MOCIE). We also appreciate Dr. N.E. Sung and Dr. M.G. Kim at the PAL for help in XAFS experiments.

References

[1] R.D. Cortright, R.R. Davda, J.A. Dumesic, Nature 418 (2002) 964–967.
[2] J. Goldemberg, Science 315 (2007) 808–810.
[3] C.N. Hamelinck, A.P.C. Faaij, Energy Policy 34 (2006) 3268–3283.
[4] R.R. Davda, J.W. Shabaker, G.W. Huber, R.D. Cortright1, J.A. Dumesic, Appl. Catal. B: Environ. 56 (2005) 171–186.
[5] P.E. Tsiakaras, J. Power Sources 171 (2007) 107–112.
[6] H. Li, G. Sun, L. Cao, L. Jiang, Q. Xin, Electrochim. Acta 52 (2007) 6622–6629.
[7] E. Antolini, J. Power Sources 170 (2007) 1–12.
[8] F.C. Simões, D.M. dos Anjos, F. Vigier, J.-M. Léger, F. Hahn, C. Coutanceau, E.R. Gonzalez, G. Tremiliosi-Filho, A.R. de Andrade, P. Olivi, et al. J. Power Sources 167 (2007) 1–10.
[9] A.O. Neto, R.R. Dias, M.M. Tusi, M. Linardi, E.V. Spinacé, J. Power Sources 166 (2007) 87–91.
[10] F. Colmati, E. Antolini, E.R. Gonzalez, Appl. Catal. B: Environ. 73 (2007) 106–115.
[11] M.J. González, C.T. Hable, M.S. Wrighton, J. Phys. Chem. B 102 (1998) 9881–9890.
[12] C. Lamy, E.M. Belgsir, J.-M. Léger, J. Appl. Electrochem. 31 (2001) 799–809.
[13] S. Song, P. Tsiakaras, Appl. Catal. B: Environ. 63 (2005) 187–193.
[14] Z. Qi, A. Kaufman, J. Power Sources 118 (2003) 54–60.
[15] W. Vielstich, A. Lamm, H.A. Gasteiger, Handbook of Fuel Cells, John Wiley & Sons, England, 2003.
[16] J.B. Goodenough, R. Manoharan, Chem. Mater. 1 (1989) 391–398.

[17] A.S. Aricó, V. Antonucci, N. Giordano, A.K. Shukla, M.K. Ravikumar, A. Roy, S.R. Barman, D.D. Sarma, J. Power Sources 50 (1994) 295–309.
[18] W.J. Zhou, S.Q. Song, W.Z. Li, Z.H. Zhou, G.Q. Sun, Q. Xin, S. Douvartzides, P. Tsiakaras, J. Power Sources 140 (2005) 50–58.
[19] J. Zeng, J. Yang, J.Y. Lee, W. Zhou, J. Phys. Chem. B 110 (2006) 24606–24611.
[20] A.S. Aricó, S. Srinivasan, V. Antonucci, Fuel Cells 1 (2001) 133–161.
[21] J. Kua, W.A. Goddard III, J. Am. Chem. Soc. 121 (1999) 10928–10941.
[22] C.D. Wagner, L.E. Davis, M.V. Zeller, J.A. Taylor, R.H. Raymond, L.H. Gale, Surf. Interface Anal. 3 (1981) 211–225.
[23] M.J. Newville, Synchrotron. Rad. 8 (2001) 322–324.
[24] B. Ravel, M. Newville, J. Synchrotron. Rad. 12 (2005) 537–541.
[25] A.L. Ankudinov, A.I. Nesvizhskii, J.J. Rehr, Phys. Rev. B 67 (2003) 115120.
[26] B.K. Teo, EXAFS:Basic Principles and Data Analysis, Springer-Verlag, Berlin, 1986.
[27] S. Mukerjee, S. Srinivasan, M.P. Soriaga, J. Mcbreen, J. Electrochem. Soc. 142 (1995) 1409–1422.
[28] S. Mukerjee, S. Srinivasan, M.P. Soriaga, J. Mcbreen, J. Phys. Chem. 99 (1995) 4577–4589.
[29] A. Borgna, S.M. Stagg, D.E. Resasco, J. Phys. Chem. B 102 (1998) 5077–5081.
[30] I.G. Casella, E. Desimoni, Electroanalysis 8 (1996) 447–453.
[31] V. Radmilović, H.A. Gasteiger, P.N. Ross Jr., J. Catal. 154 (1995) 98–106.
[32] V. Radmilovic, T.J. Richardson, S.J. Chen, P.N. Ross Jr., J. Catal. 232 (2005) 199–209.
[33] A.R. Denton, N.W. Ashcroft, Phys. Rev. A 43 (1991) 3161–3164.
[34] S.M. Stagg, C.A. Querini, W.E. Alvarez, D.E. Resasco, J. Catal. 168 (1997) 75–94.
[35] M. Peuckert, H.P. Bonzel, Surf. Sci. 145 (1984) 239–259.
[36] A.I. Frenkel, C.W. Hills, R.G. Nuzzo, J. Phys. Chem. B 105 (2001) 12689–12703.
[37] T.L. Barr, J. Phys. Chem. 82 (1978) 1801–1810.
[38] G. Neri, C. Milone, S. Galvagno, A.P.J. Pijpers, J. Schwank, J. Appl. Catal. A: Gen. 227 (2002) 105–115.
[39] G.T. Baronetti, S.R. de Miguel, O.A. Scelza, A.A. Castro, Appl. Catal. 24 (1986) 109–116.
[40] J. Llorca, N. Homs, J.G. Fierro, J. Sales, P.R. Piscina, J. Catal. 166 (1997) 44–52.
[41] R.A.V. Santen, W.M.H. Sachtler, J. Catal. 33 (1974) 202–209.
[42] M. Peuckert, F.P. Coenen, H.P. Bonzel, Electrochim. Acta 29 (1984) 1305–1314.
[43] S. Biallozor, A. Kupniewska, V. Jasulaitene, Fuel Cells 3 (2003) 8–14.
[44] N. Furaya, S. Motoo, J. Electroanal. Chem. 98 (1979) 195–202.
[45] M.M.P. Janssen, J. Moolhuysen, Electrochim. Acta 21 (1976) 861–868.
[46] A.N. Haner, P.N. Ross, J. Phys. Chem. 95 (1991) 3740–3746.
[47] Y. Ishikawa, M.-S. Liao, C.R. Carbera, Surf. Sci. 463 (2000) 66–80.
[48] M. Kubota, Inorg. Chem. 29 (1990) 574–576.
[49] F.B. Passos, M. Schmal, M.A. Vannice, J. Catal. 160 (1996) 106–117.
[50] R. Burch, L.C. Garla, J. Catal. 71 (1981) 348–359.
[51] F.M. Dautzenberg, J.N. Helle, P. Biloen, W.M.H. Sachtler, J. Catal. 63 (1980) 119–128.
[52] G. Meitzner, G.H. Via, F.W. Lytle, S.C. Fung, J.H. Sinfelt, J. Phys. Chem. 92 (1988) 2925–2932.
[53] E. Antolini, Appl. Catal. B: Environ. 74 (2007) 324–336.
[54] R. Alcalá, M. Mavrikakis, J.A. Dumesic, J. Catal. 218 (2003) 178–190.
[55] W.J. Zhou, Z.H. Zhou, S.Q. Song, W.Z. Li, G.Q. Sun, P. Tsiakaras, Q. Xin, Appl. Catal. B 46 (2003) 273–285.
[56] W.J. Zhou, S.Q. Song, W.Z. Li, G.Q. Sun, Q. Xin, S. Kontou, K. Poulianitis, P. Tsiakaras, Solid State Ionics 175 (2004) 797–803.
[57] R. Burch, L.C. Garla, J. Catal. 71 (1981) 360–372.
[58] R. Parsons, T. VanderNoot, J. Electroanal. Chem. 257 (1988) 9–45.
[59] K. Balakrishnan, J. Schwank, J. Catal. 127 (1991) 287–306.
[60] J.K. Norskov, C.H. Christensen, Science 312 (2006) 1322–1323.
[61] J. Greeley, M. Mavrikakis, J. Am. Chem. Soc. 126 (2004) 3910–3919.
[62] F. Delime, J.-M. Léger, C. Lamy, J. Appl. Electrochem. 29 (1999) 1249–1254.